Geosci. Model Dev. Discuss., 6, 6775–6834, 2013
www.geosci-model-dev-discuss.net/6/6775/2013/
doi:10.5194/gmdd-6-6775-2013

Geoscientific Model Development Discussions
Open Access

Radiation sensitivity tests of the HARMONIE 37h1 NWP model

K. P. Nielsen[1], **E. Gleeson**[2], **and L. Rontu**[3]

[1]Danish Meteorological Institute, Lyngbyvej 100, 2100, Copenhagen Ø, Denmark
[2]Met Éireann, Glasnevin Hill, Dublin 9, Ireland
[3]Finnish Metorological Institute, Erik Palménin Aukio 1, 00560 Helsinki, Finland

Received: 25 October 2013 – Accepted: 29 November 2013 – Published: 17 December 2013

Correspondence to: K. P. Nielsen (kpn@dmi.dk)

Published by Copernicus Publications on behalf of the European Geosciences Union.

Abstract

It is essential to be able to identify which element of a numerical weather prediction (NWP) model or climate model causes biases in the model output compared with observations. With respect to shortwave (SW) radiation fluxes many elements affect the final results. Here we present a focussed study of the SW radiation schemes in the HARMONIE NWP model. Detailed calculations have been made with the DISORT model run in the libRadtran framework. These are used as a benchmark against which the NWP radiation calculations can be tested. Both models are given the same atmospheric properties as input. Several configurations of the IFS radiation scheme and the hlradia radiation schemes have been tested. The usefulness of the benchmarking tests is demonstrated and concrete strength and weaknesses of the radiation schemes are elucidated. The benchmark data may be used for testing radiation schemes in other NWP or climate models.

1 Introduction

One of the main problems in comparing numerical weather prediction (NWP) models to observations, is that there is generally a long chain of elements in the models that leads to the given results. This is also true for modelled solar radiation fluxes. Correctly modelling these depends firstly on correctly describing the state of the atmosphere and the surface. In particular cloud liquid water and cloud ice concentrations are important, but cloud droplet number concentration, cloud ice particle concentration, cloud ice particle shape and size distributions, water vapour, aerosols, ozone, surface reflectance, Sun-Earth distance, air pressure, altitude and position of Sun relative to the given topography can also significantly affect the net and downward global radiation (Sagan and Pollack, 1967; Hansen and Travis, 1974; Pierluissi and Peng, 1985; Shettle, 1989; Hu and Stamnes, 1993; Fu, 1996; Hess et al., 1998; Thomas and Stamnes, 2002; Reddy et al., 2005; Forster et al., 2007; Myhre et al., 2007; Senkova et al., 2007;

GMDD
6, 6775–6834, 2013

Kahnert et al., 2008; L'Ecuyer et al., 2008; Manners et al., 2012). Secondly, when the atmospheric state is known, the optical properties of particles and gases in the atmosphere need to be correctly calculated. Thirdly, a sufficiently accurate radiative transfer scheme is needed to estimate the solar radiation fluxes.

Here we focus on the second and third steps described above, by testing various radiation parametrizations, available in the HIRLAM Aladin Regional Mesoscale Operational NWP In Europe (HARMONIE) NWP model, against the accurate one-dimensional radiative transfer model, DISORT (Stamnes et al., 1988, 2000) in prescribed atmospheric conditions. DISORT is run within the framework of the libRadtran library (Mayer and Kylling, 2005).[1] The aim of our study is to understand the differences between the available radiation parametrizations in terms of the solar (shortwave, SW) radiation fluxes compared to an accurate reference. The results of such a comparison will indicate where the NWP SW radiation parametrizations need improvement.

Oreopoulos et al. (2012) have recently compared a large set of SW and longwave radiation schemes that are currently used in atmospheric models. In their test, realistic atmospheric profiles from the Atmospheric Radiation Measurement programme were used. Here we use idealised cases which are not necessarily realistic. The advantage of using idealised cases is that the full range of sensitivity can be tested for each of the relevant variables individually. Fixed atmospheric states and surface properties are used both in HARMONIE and in DISORT.

The HARMONIE NWP system combines elements from the global IFS/Arpege model (Déqué et al., 1994) with the ALADIN nonhydrostatic dynamics (Bénard et al., 2010) and physical parametrizations of AROME (Seity et al., 2011) and HIRLAM (Undén et al., 2002). In the current version (37h1), the default SW radiation scheme is based on the IFS radiation transfer code (IFS cycle 25R1, European Centre for Medium-Range Weather Forecast implementation in 2002), see ECMWF (2012) and Mascart and Bougeault (2011). This is a comprehensive, but also computationally demanding, scheme with several spectral bands both in the solar and terrestrial radiation

[1] www.libradtran.org

GMDD
6, 6775–6834, 2013

ranges. In the following, we refer to this as the IFS radiation scheme. Here we test this scheme and also the alternative HIRLAM radiation scheme, further denoted as hlradia, which is based on Savijärvi (1990). Hlradia is an alternative simple and fast radiation parametrization. In hlradia, the cloud transmittance and cloud absorptance is calculated with the parametrization of Wyser et al. (1999).

In practice, a simple radiation scheme applied at each time-step (currently 1 minute) of the model integration requires as much computation time as a complicated scheme called a few times in a hour. The accuracy requirements for radiation parametrizations in long-term climate simulations on relatively coarse spatial and temporal scales differ from those of the kilometre-scale short-term NWP models run in continuous data assimilation forecast cycles. For example, the importance of quickly changing cloud-radiation interactions may be greater in the latter while the former requires maximum accuracy in handling the details of gaseous transmission. It is thus of interest to understand and compare the accuracy of the simple and complex schemes against a good reference. Such a reference for testing the HARMONIE SW radiation parametrizations was obtained by applying the DISORT model. The benchmark computations done by the detailed radiative transfer model also provide valuable information about the sensitivity of SW radiation fluxes to a wide range of various atmospheric properties.

2 Methods

Different SW radiation schemes currently available in the HARMONIE framework were compared with DISORT results for 12 experiments. The experiments can be split into three groups: clear sky experiments 1–4, liquid cloud experiments 5–8, and ice cloud experiments 9–12. In each of the experiments the sensitivity to a different variable was studied as outlined in Table 1.

The DISORT algorithm was run in the spectral range 280 nm to 3001 nm with 1 nm resolution and an angular discretisation of 30 streams. The Kurucz (1992) solar spectrum averaged to 1 nm resolution by Bernhard Mayer was used as input.

GMDD
6, 6775–6834, 2013

The HARMONIE default IFS radiation scheme has six SW spectral bands: 3 bands in the ultraviolet and visible spectral ranges and 3 bands in the solar infrared spectral range. Specifically, these six spectral bands are defined by the wavelengths: 0.185–0.25–0.44–0.69–1.19–2.38–4.00 µm (Mascart and Bougeault, 2011). The radiative transfer calculations are done using the delta-Eddington approximation (Joseph et al., 1976; Fouquart and Bonnel, 1980). In HARMONIE version 37h1, the default cloud liquid optical properties for the IFS scheme are calculated with the Fouquart (1987) parametrization. It is also possible to use the Slingo (1989) parametrization. The cloud ice optical properties are calculated with the Ebert and Curry (1992) parametrization. Alternatively, the Fu (1996) parametrization can be used. Here we test each of these four cloud optical property options.

Additionally, we propose a new cloud liquid optical property scheme (hereafter, referred to as the Nielsen scheme) based on the Mie solution to Maxwell's equations (Mie, 1908; Wiscombe, 1980) for each of the 6 SW spectral bands used in the HARMONIE IFS scheme. The new parametrization is described in Eqs. (3)–(5) and in Table 2. In the IFS radiative transfer calculations the key input variable is the scaled optical depth τ_i^*, which is a product of the optical depth τ_i and the delta-Eddington scaling factor $(1 - \omega_i g_i^2)$ (Joseph et al., 1976):

$$\tau_i^* = (1 - \omega_i g_i^2)\tau_i \quad (1)$$

$$\tau_i = \beta_i C, \quad (2)$$

where, according to the suggested new scheme,

$$\beta_i = a_i r_{\mathrm{e,\,liq}}^{-b_i} \quad (3)$$

$$\omega_i = c_i - d_i r_{\mathrm{e,\,liq}} \quad (4)$$

$$g_i = e_i + f_i r_{\mathrm{e,\,liq}} - h_i \exp(-j_i r_{\mathrm{e,\,liq}}) \quad (5)$$

Here, i denotes the wavelength band index, ω_i is the single scattering albedo, g_i is the asymmetry factor, β_i is the mass extinction coefficient in $\mathrm{m^2\,g^{-1}}$ and C is the mass load

GMDD
6, 6775–6834, 2013

in $g\,m^{-2}$, $r_{e,\,liq}$ is the cloud droplet effective radius, and a_i, b_i, c_i, d_i, e_i, f_i, h_i and j_i are coefficients as detailed in Table 2.

As can be seen in Eq. (2), the asymmetry factor g_i is important for the scaling factor. For this reason we have made a more comprehensive empirical formula for g_i in Eq. (5) than those used in the Fouquart (1987) parametrization and in the Slingo (1989) parametrization, where g_i is given as constants in the former and as linear functions of r_e in the latter.

Notice that the parametrization for wavelength band 1 (0.185–0.25 µm) is irrelevant, as virtually no SW irradiance at these wavelengths reaches the levels of the lower atmosphere, where clouds occur. This is why it is omitted in Table 2.

A slightly modified version of hlradia was also available for our tests in the HARMONIE framework. In hlradia one SW spectral band is considered and both the clear sky and cloudy sky transmittances and absorptances are parametrized in order to make the scheme very fast (Savijärvi, 1990; Wyser et al., 1999). In hlradia the impact of ozone, oxygen and carbon dioxide, as well as aerosols, on SW irradiance is assumed to be constant over time and space.

MUSC, the single column version of HARMONIE, based on Malardel et al. (2006), was used as a framework to provide the radiation schemes with the atmospheric and surface input data. A vertical resolution of 41 full model levels (in hybrid coordinates) between the surface and an elevation of 52 km was used (Undén, 2010). The same model levels were used in the DISORT calculations. Only output from the first time-step of MUSC was used in order to exclude the influence of an evolving atmospheric state on the results.

The reference (initial) definitions for the HARMONIE and DISORT experiments are:

- Day of year = 79, i.e. 20 March or vernal equinox
- Altitude = 0.0 km a.s.l.
- Solar zenith angle = 56°

GMDD
6, 6775–6834, 2013

- Surface albedo = 0.18
- Clear sky
- "Mid-latitude summer" atmospheric profile from Anderson et al. (1986), including geopotential heights, temperature, air densities, mixing ratios of water vapour, ozone, oxygen and carbon dioxide from the surface to the top of the atmosphere assumed to be at 120 km.
- Integrated water vapour load = 29.63 kg m^{-2} (Anderson et al., 1986).

Water vapour input data were interpolated to the model levels, keeping the vertical distribution unchanged when modifying the vertically integrated load in the experiments.

In order to make the sensitivity experiments as simple as possible, all clouds were assumed to be homogeneous and to be situated between 1 km and 2 km above the surface and to have prescribed properties. Such clouds may be completely unrealistic and in contradiction to the assumed water vapour distribution. However, our aim here is not to make realistic experiments, but rather to make a focussed test of the radiative transfer parametrizations in HARMONIE. Using idealised clouds also enables us to test a wider variety of cloud types than if we, for instance, had used cloud data from measurement campaigns.

Aerosols are described differently in each of the three radiation schemes: in libRadtran/DISORT the Shettle (1989) rural aerosol profile is used, in the HARMONIE IFS scheme an aerosol climatology (Tanré et al., 1984; Mascart and Bougeault, 2011) is applied and in hlradia aerosols are represented by constant coefficients (Savijärvi, 1990). As these cannot be compared in detail, i.e. for various aerosol types and concentrations, we only compare the effect of including and excluding aerosols in each scheme (experiment 3).

GMDD
6, 6775–6834, 2013

3 Results and discussion

In the following sub-sections the total downward SW irradiance at the surface on a horizontal plane, i.e. the global radiation [$\mathrm{W\,m^{-2}}$], is presented for each of the 12 radiation sensitivity experiments (Table 1). In addition, net fluxes on model levels are presented for a select number of the experiments. Net fluxes, defined as the downward SW fluxes minus the upward SW fluxes, are presented as % differences relative to the accurate DISORT model. Clear sky experiments are discussed in Sect. 3.1 and cloud liquid and cloud ice experiments are discussed in Sects. 3.2 and 3.3, respectively. In these experiments when the cloud condensate is $> 0\,\mathrm{kg\,m^{-2}}$ the fractional cloud cover was set to 1.

3.1 Clear sky experiments

Four clear sky experiments were carried out to test the SW radiation sensitivity to water vapour (experiment 1), solar zenith angle (experiment 2), aerosols (experiment 3) and surface albedo (experiment 4).

3.1.1 Experiment 1: water vapour

In the water vapour experiment (experiment 1), the agreement between the IFS radiation scheme and DISORT is within 1 % for the global radiation while the hlradia shows a consistent positive bias of 4 % to 6 % or $30\,\mathrm{W\,m^{-2}}$ to $40\,\mathrm{W\,m^{-2}}$ relative to DISORT (Fig. 1). The absolute and relative biases of hlradia increase with decreasing water vapour mixing ratio. The height level net flux deviation of IFS from DISORT (Fig. 2) varies from approximately +2.5 % at the top of the atmosphere to between −0.5 % and −1.0 % at the surface. By studying both the upward and downward flux components of IFS and DISORT (not shown here), we find that the difference at the top of the atmosphere comes primarily from differences in the downward component of the fluxes.

GMDD
6, 6775–6834, 2013

The hlradia net flux differences are approximately +1.0 % at the top of the atmosphere increasing towards +5.0 % at the surface (Fig. 3). For hlradia, it is not possible to separate the model level downward and upward radiation fluxes. Thus, the positive bias in the net SW flux, which increases towards the surface may be due to an overestimation of the downward or an underestimation of the reflected radiation. In both cases, the most humid near-surface layers seem to systematically transmit more and absorb less SW radiation in hlradia than in the reference DISORT.

Gases other than water vapour affect the SW radiation. The most important of these is ozone. We have tested the SW sensitivity to ozone by running DISORT. Here the ozone cross section parametrization of Bass and Paur (1985) is used. When ozone was reduced from 500 Dobson Units (DU) to 100 DU, the global radiation at the surface increased by 2.3 %. Since 500 DU and 100 DU are extreme values of the ozone layer thickness, we find that there is little error in using climatological ozone data (as is done in the IFS radiation scheme), or in using constant ozone SW absorption (as is done in hlradia). In an hlradia experiment, a complete removal of the ozone absorption led to an increase in the global radiation at the surface of 4.5 %. Detailed UVB/UVA estimations are not needed in general NWP computations and should be done separately by combining the modelled SW fluxes with the most recent ozone measurements.

The variations in carbon dioxide and oxygen are practically irrelevant for SW radiation in NWP modelling, because they only affect the extreme fringes of the IR and UV parts of the solar spectrum, respectively. As an example we tested the sensitivity of SW radiation to carbon dioxide concentration with DISORT. The carbon dioxide concentration is set to 330 ppm in the "mid-latitude summer" profile from Anderson et al. (1986). In both IFS and hlradia, this is set to be 353 ppm. Increasing the carbon dioxide concentration in the DISORT run from 330 ppm to 353 ppm causes a relative decrease of 0.01 % in the surface downward global SW radiation. The relative impact of changing the oxygen concentation on the surface downward global SW radiation is even less. In an hlradia experiment, the effect of doubling the CO_2 concentration on the SW radiation fluxes was not detected.

GMDD
6, 6775–6834, 2013

3.1.2 Experiment 2: solar zenith angle

The solar zenith angle (SZA) experiment (experiment 2, Fig. 4) shows agreement between the IFS global radiation and DISORT to within 1.5 % for most SZAs. However, when SZA = 80° (low solar elevation) the DISORT global radiation is 16 % lower than that from the IFS radiation scheme. Large relative differences are also present in the case of the hlradia scheme for the largest SZA. For the higher SZAs the relative difference for hlradia increases from +1.6 % for SZA = 0° to +5.3 % for SZA = 60°. However, in terms of the absolute differences, the IFS global radiation is always within ±20 $\mathrm{W\,m^{-2}}$ of the DISORT results, while hlradia again shows a systematic overestimation of +15 to +25 $\mathrm{W\,m^{-2}}$, which is consistent with Fig. 1 for the case where the reference water vapour load is equal to that used in the SZA experiment (29.63 $\mathrm{kg\,m^{-2}}$).

For the largest SZAs the DISORT results are not accurate for two reasons. Firstly, the atmosphere is assumed to consist of plane parallel layers (Stamnes et al., 1988), whereas in reality the atmosphere consists of spherical shells. This causes a negative error, since the atmospheric optical depth is overestimated. Secondly, the illumination is assumed to be plane parallel, whereas the Sun has an angular extension of 0.5°. At a SZA of 80° this has been shown to cause a positive error of 2.5 % (Stamnes et al., 2000). In the IFS radiation scheme the sphericity of the atmosphere is accounted for with the magnification factor of Rodgers (1967):

$$\mu_{0,\,\mathrm{corrected}} = \frac{\sqrt{1224\mu_0^2 + 1}}{35}, \tag{6}$$

where μ_0 is the cosine of the SZA. In the empirical SW clear sky transmittance formula in hlradia, there is no explicit correction done to account for the sphericity of the atmosphere (Savijärvi, 1990).

GMDD
6, 6775–6834, 2013

3.1.3 Experiment 3: with and without aerosols

Experiment 3 involved testing aerosols, i.e. the atmospheric particles, which are treated differently in each of the schemes. Each scheme was tested with and without the inclusion of aerosols. It can be seen from Table 3 that including aerosols in the radiation schemes causes a decrease of between 25 $W m^{-2}$ and 40 $W m^{-2}$ in the global radiation depending on which scheme is used. Comparing the schemes, the HARMONIE IFS scheme agrees with DISORT to within ±1.5 %, while the hlradia scheme shows relative differences of between +4 % and +6 %. When aerosols are included, the relative difference between the IFS scheme and DISORT is −1.0 %. The overestimation of global radiation by hlradia compared to DISORT is quite similar for the cases with and without aerosols (4.5 % and 5.5 % respectively), which again points towards the handling of water vapour transmission as the main source of the clear sky SW radiation bias in hlradia.

3.1.4 Experiment 4: surface albedo – clear sky case

In experiment 4 the sensitivity of varying the surface albedo in clear sky conditions was tested (Fig. 5). Once again, the relative difference for the IFS radiation scheme compared to DISORT is very low, ranging from −0.5 % to −1 %. For the hlradia radiation scheme the relative differences range from +4 % to +5 %, increasing with increasing albedo. The differences in net fluxes as a function of height in the atmosphere are shown in Figs. 6 and 7 for the IFS and the hlradia radiation schemes, respectively, relative to DISORT. The differences in the net fluxes are less than 1 % at the surface for the IFS radiation scheme and increase with increasing surface albedo to up to 20 % at a height of 2–3 km. The differences in net fluxes for the hlradia radiation scheme are less than +5 % at the surface and decrease to less than −5 % in the upper atmosphere for the higher surface albedos.

GMDD
6, 6775–6834, 2013

3.2 Liquid cloud experiments

Four liquid cloud experiments were run to test the SW radiation sensitivity to cloud water load, cloud drop effective radius ($r_{e,\,liq}$) and surface albedo. Tests of the surface albedo sensitivity were run for both the case of a cloud of medium thickness (cloud water load 0.1 $kg\,m^{-2}$) and the case of a thick cloud (cloud water load 1.0 $kg\,m^{-2}$).

3.2.1 Experiment 5: cloud water load

Experiment 5 was run to test the cloud water load sensitivity. A fixed $r_{e,\,liq}$ of 10 µm was used, which is a typical value for stratocumulus clouds (e.g. Martin et al., 1994).

Before being used for SW radiation calculations the cloud water load is modified by a so-called cloud SW inhomogeneity factor of 0.7 in the default SW scheme of HARMONIE 37h1. In hlradia, an SW inhomogeneity factor of 0.8 is used as default. After several tests, it became clear that the SW inhomogenity factor is very significant. We therefore performed an additional test. In Fig. 8 and in Table 4 the effect of changing the inhomogeneity factor can be seen.

For cloud water loads of 0.05 $kg\,m^{-2}$ to 0.1 $kg\,m^{-2}$ the transmitted global radiation is almost 50 $W\,m^{-2}$ higher with the SW inhomogeneity factor set to 0.7, as compared to when it is set to 1.0, for the case where the default Harmonie radiation settings are used i.e. IFS with the Fouquart cloud optical property parametrization (Fouquart, 1987). Similarly, when the hlradia scheme is used with an SW inhomogeneity factor of 1.0 rather than 0.8, the global radiation is more than 30 $W\,m^{-2}$ less. Note that in our experiments, where cloud water load is given as an input value, application of an inhomogeneity factor means reduction of this predefined input with 20 % (hlradia) or 30 % (IFS).

Overall, when the cloud SW inhomogeneity factor is set to 1.0, the results are closer to those from DISORT. This is not surprising, as the DISORT benchmark tests were done for horizontally homogeneous clouds. In both the Meso-NH model (Mascart and Bougeault, 2011) and in the most recent cycles of the global IFS model (ECMWF,

GMDD
6, 6775–6834, 2013

2012) the cloud SW inhomogeneity factor is set to 1.0. Some meteorological institutes run hlradia (within the operational HIRLAM) with this setting. In all of the following cloud experiments (5–12) we set the cloud inhomogeneity factor to 1.0 for every scheme. In Sect. 3.2.2 we discuss the cloud SW inhomogeneity at a more general level.

The discrepancies between using the IFS radiation scheme with the HARMONIE 37h1 default cloud liquid optical property scheme (Fouquart, 1987), hlradia and the accurate DISORT model are shown in Fig. 9. In this figure the results obtained when using two alternative liquid cloud optical property schemes are also shown. The first of these schemes is the Slingo (1989) scheme that is optionally available in HARMONIE 37h1, while the second is the Nielsen scheme as described in Eqs. (3–5) and Table 2. In Table 5 the results are shown in the form of absolute differences compared to the DISORT calculations.

It can be seen that the default IFS radiation scheme in HARMONIE, with the Fouquart (1987) liquid cloud optical property scheme, shows a positive bias of up to $+32\,\mathrm{W\,m^{-2}}$ (+8 %) for clouds with $0.02\,\mathrm{kg\,m^{-2}}$ cloud water load but shows a smaller bias for more water-rich clouds. For the alternative Slingo (1989) liquid cloud optical property scheme the results show a negative bias of up to $-34\,\mathrm{W\,m^{-2}}$ (−17 %) for clouds with a $0.1\,\mathrm{kg\,m^{-2}}$ cloud water load. The Nielsen liquid cloud optical property scheme has the lowest overall bias in this experiment, with a maximum bias of $-17\,\mathrm{W\,m^{-2}}$ (−8 %) for a cloud water load of $0.1\,\mathrm{kg\,m^{-2}}$. For the hlradia scheme there is a high positive bias of up to $+53\,\mathrm{W\,m^{-2}}$ (+11 %) for a cloud water load of $0.005\,\mathrm{kg\,m^{-2}}$. For cloud water loads of $0.1\,\mathrm{W\,m^{-2}}$ and higher, the hlradia scheme has practically no bias. Here the positive bias of the hlradia scheme in clear sky conditions (Figs. 1, 3, 4, 5 and 7) should be kept in mind. If this were to be corrected, the hlradia results overall would be around 5 % lower in this experiment.

In Figs. 10–13 the relative differences between the net fluxes as a function of height are shown for each of the four parametrizations tested. As for the global radiation, the net fluxes mostly have a positive bias both below and above the clouds when the Fouquart parametrization is used an increasingly negative bias is seen below

GMDD
6, 6775–6834, 2013

increasingly thicker clouds (Fig. 10). For the Slingo and Nielsen parametrizations the significant negative biases in the net fluxes are predominantly below the clouds, while the differences are smaller and mostly positive above the clouds (Figs. 11 and 12). Again an increasingly negative bias is seen below increasingly thicker clouds. The results for the hlradia scheme do not display this pattern (Fig. 13). Instead, a clear negative bias ($< -20\,\%$) is seen in the net flux only at the top of the thicker clouds, but not below and above these. Such a pattern can be explained by a too large cloud absorptance and a too low cloud reflectance in the hlradia scheme.

3.2.2 General discussion on cloud inhomogeneity

In an NWP model grid box clouds may be inhomogeneously distributed. It can easily be shown that representing clouds as a linear average covering a certain fraction of the grid box does not produce the same SW transmittance and reflectance as when the clouds are resolved. This is because the cloud transmittance and reflectance do not vary linearly with cloud optical depth. On the other hand, in cases where clouds are homogeneously distributed within a gridbox the linear average is correct. Therefore, it is incorrect to multiply clouds in *all* grid boxes by the same cloud inhomogeneity factor, as is currently done in HARMONIE. To deal with these issues properly, and also to deal with the effects of 3-D cloud radiation transfer, more a sophisticated scheme like the one recently proposed by Hogan and Shonk (2013) is required.

3.2.3 Experiment 6: cloud drop effective radius

Experiment 6 was run to study the sensitivity of the schemes to varying $r_{\mathrm{e,\ liq}}$, keeping the integrated cloud water load at $0.1\,\mathrm{kg\,m^{-2}}$. The global radiation results are shown in Fig. 14 and in Tables 6 and 7. The net irradiance results relative to DISORT are shown in Figs. 15–18.

The new Nielsen parametrization clearly performs best compared to the DISORT calculations (Fig. 14 and Tables 6–7). The Slingo parametrization performs considerably

GMDD
6, 6775–6834, 2013

worse when $r_{e,\,liq}$ is varied, which is in contrast to experiment 5 where the liquid cloud water load was varied (Fig. 9). This parametrization was designed for a limited cloud droplet size range of 4.2–16.6 µm (Slingo, 1989). Therefore, it is not surprising that its performance deteriorates for large cloud droplet sizes. Previously, Dobbie et al. (1999) have shown that the Slingo parametrization does not agree with calculations based on Mie theory for the larger cloud droplets. The Fouquart parametrization has a consistently positive bias as a function of $r_{e,\,liq}$ relative to DISORT (+15 W m^{-2} to +25 W m^{-2} i.e. +6 % to +17 %). The hlradia parametrization performs very well for the small cloud droplets but has a positive bias for cloud droplets which are larger than 15 µm.

In Figs. 15–18 the corresponding results for the net flux differences are shown. Again, the positive bias in the net fluxes is consistently positive for all height levels when the Fouquart parametrization is used (Fig. 15). The biases of the Slingo (Fig. 16) and Nielsen (Fig. 17) schemes are mainly below the cloud rather than above. For the Nielsen scheme the negative bias increases with decreasing $r_{e,\,liq}$. As in Fig. 14, the results for the hlradia scheme are very good (Fig. 18) also for the atmospheric net fluxes.

3.2.4 Experiments 7 and 8: surface albedo under liquid cloud conditions

Experiment 7 was run for a fixed integrated cloud water load of 0.1 kg m^{-2} and a fixed $r_{e,\,liq}$ of 10 µm. The results of varying the surface albedo can be seen in Fig. 19, which shows that the three cloud optical property parametrizations in the IFS scheme have similar sensitivities to surface albedo. The increase in global radiation as a function of surface albedo is slightly greater in the case of hlradia. When DISORT is used the increase in global radiation as a function of the surface albedo is larger than for each of the HARMONIE schemes.

Experiment 8 was run for a fixed integrated cloud water load of 1.0 kg m^{-2} and was otherwise similar to experiment 7. As in experiment 7, it can be seen that the global radiation sensitivity in DISORT as a function of the surface albedo is considerably larger than for the HARMONIE cases (Fig. 20).

GMDD
6, 6775–6834, 2013

In each of the experiments the surfaces were assumed to have angular distributions of scattering that follow Lambert's cosine law (Lambert, 1760). In reality, such surfaces do not exist (Lommel, 1889; Bhandari et al., 2011), but they are used in NWP and climate models due to the lack of computational resources needed to resolve the angular radiance distribution. In the 30-stream DISORT simulations the angular radiance distribution is resolved, but since the assumption of Lambertian surface reflectance is made, the surface reflectance cannot be the reason for the discrepancies seen in Figs. 19 and 20. The differences must thus arise from differences in the downward global radiation. The sensitivity of this to the surface albedo arises from multiple reflections of the SW irradiance between the surface and the cloud layer.

In the IFS scheme all scattered irradiance, including that transmitted diffusely through clouds, is modelled as having a zenith angle of 53.0°, i.e. the irradiance transmitted diffusely through or reflected from clouds is assumed to be on average 60 % (i.e $\cos(53.0^\circ)$) of the irradiance normal to the surface (Mascart and Bougeault, 2011). An assumption like this is necessary in the delta-Eddington scheme or any scheme that does not resolve the angular distribution of the radiance (Thomas and Stamnes, 2002).

Hopf (1936) showed that the effective angle of irradiance transmitted diffusely through an optically thick conservatively scattering medium approaches 45° as the optical depth approaches infinity. Thus, 71 % of the irradiance reaches a horizontal surface compared to the case where all the irradiance is normal to the surface. This relative amount of irradiance as a function of optical depth is referred to as the *Hopf q function*. The value $q(\infty) = 71\,\%$ is almost reached at an optical depth of 1.5, where $q(1.5)$ is 70.5 % as shown by King (1960) and King et al. (1965). Thus, for optical depths of 1.5 and above the diffuse transmittance of SW irradiance through thick clouds is underestimated by approximately 18 % in the IFS scheme.[2]

[2]The relation between the optical depth, cloud water load and $r_{e,\,liq}$ can be calculated based on Eqs. (1)–(5). For example, the optical depth of 1.5 in case of the third spectral band would correspond to the cloud liquid water load of approximately 9.6 g m^{-2} when $r_{e,\,liq}$ is 10 µm.

GMDD
6, 6775–6834, 2013

When the optical depth is 0, the Hopf q function is 57.7 %, which is close to the value assumed in the IFS-radiation scheme. Thus, it seems very likely that the assumptions about the Hopf q function in the IFS-scheme is the cause of the increasingly negative biases below increasingly optically thick clouds, as seen for example in Figs. 12 and 17. It also seems reasonable that the significance of this is amplified below clouds where there are multiple reflections due to a high surface albedo. In order to test this hypothesis we ran an additional version of experiment 5 with a changed Hopf q function in the IFS scheme. The results of setting the Hopf q function to 71 % can be seen in Fig. 21, which should be compared with Fig. 12, where the IFS default Hopf q function value of 60 % was used.

This extra experiment illustrates the significance of the Hopf q function. The negative bias under the thicker liquid clouds is reduced, while there is an increased positive bias under the thinner liquid clouds and above the cloud layer. This shows that a Hopf function that varies with the optical properties in the atmosphere should be used rather than a constant value, which will not be correct in all cases. Implementing a variable Hopf function in the IFS scheme could be a computationally cheap way of improving the radiative transfer calculations.

3.3 Ice cloud experiments

Four ice cloud experiments were run to test the SW radiation sensitivity to cloud ice load and cloud ice particle equivalent radius ($r_{\mathrm{e,\ ice}}$) in the case of a typical land surface albedo of 0.18 and a typical snow surface albedo of 0.7. Experiments 9 and 10 were run for a fixed $r_{\mathrm{e,\ ice}}$ of 50 µm. This is a typical value of $r_{\mathrm{e,\ ice}}$ for pure ice clouds (Fu, 1996; Nielsen, 2011).

3.3.1 Experiments 9 and 10: cloud ice load

For the IFS radiation scheme, we tested the Fu and Liou (1993) ice cloud parametrization, which is the default in Harmonie 37h1, and the more recent Fu (1996)

GMDD
6, 6775–6834, 2013

parametrization. As can be seen in Fig. 22 both of these parametrizations compare very well to the DISORT calculations in the cloud ice load sensitivity test with low albedo (experiment 9). In the high albedo case (experiment 10) both parametrizations show a significant negative bias for cloud ice loads of 0.2 $\mathrm{kg\,m^{-2}}$ and above as shown in Fig. 23. Both the Fu and the Fu–Liou schemes perform excellently in experiment 9 and very well for most cloud ice loads in experiment 10. The hlradia scheme performs worse than the IFS schemes. Again, this can to a large extent be explained by the clear sky positive bias of hlradia. With the clear bias removed, the hlradia results in experiments 9 and 10 (Figs. 22 and 23) would be around 5 % lower and much closer to the IFS scheme results. This also applies to experiments 11 and 12 (Figs. 24 and 25).

3.3.2 Experiments 11 and 12: cloud ice particle equivalent radius

In Figs. 24 and 25 the results from the two tests of SW sensitivity to $r_{\mathrm{e,\ ice}}$ are shown. It can be seen that the Fu (1996) parametrization shows better agreement with the DISORT calculations than the Fu and Liou (1993) parametrization. Both of these show a negative bias of approximately −10 % for the smallest $r_{\mathrm{e,\ ice}}$ in the low and high surface albedo cases (Figs. 24 and 25).

In Figs. 26–28 the net flux differences relative to DISORT are shown for the Fu and Liou (1993) parametrization, the Fu (1996) parametrization and the hlradia scheme (Wyser et al., 1999), respectively. For the latter a strong positive bias is seen in the net fluxes at all atmospheric levels. In the two first cases the largest biases are seen under the clouds with the largest cloud ice loads. This is a similar pattern to that seen in the cloud liquid water load tests (Figs. 11 and 12), which again supports our hypothesis that the Hopf q function should be a function of optical depth in the radiation scheme.

In both DISORT, IFS and hlradia cloud ice is considered to consist of hexagonal crystals. In reality, cloud ice particles come in multiple shapes (Baker and Lawson, 2006; Lawson et al., 2006). As shown by Kahnert et al. (2008), these shapes significantly affect the SW forcing of the cloud. Thus, the benchmarking quality of the DISORT run, in

GMDD
6, 6775–6834, 2013

this case, is no better than the correctness of the basic assumption made on the cloud ice particle shape. It is only correct for ice clouds consisting of hexagonal crystals.

4 Conclusions and outlook

Overall we have demonstrated an effective method for testing the radiative transfer computations performed in an NWP model. By defining simplified atmospheric and surface conditions in a single-column model, we have full control of the input and can make clean comparisons of the different parametrizations. Such baseline testing is a necessary first step towards studying the sensitivity of NWP model results – the weather forecast – to the radiation parametrizations, for which integration in time in a realistic evolving 3-D atmospheric environment is required. We have found strengths and weaknesses of the IFS and hlradia parametrizations in HARMONIE in the controlled experiments and suggest the improvements outlined below.

Regarding the IFS SW radiation scheme with HARMONIE default settings in comparison to highly detailed radiative transfer calculations we found that:

- The clear sky computations compare excellently.
- The Fu (1996) cloud ice optical property parametrization compares better than the Fu and Liou (1993) parametrization. However, both compare fairly well, given the assumption that cloud ice particles are hexagonal columns.
- A new optical property parametrization for liquid clouds has been developed. We have shown that this is better than the parametrizations currently available in HARMONIE.
- Assuming climatological ozone profiles induces an SW error of a few percent at most.

Regarding the much simpler hlradia SW scheme with only one spectral band we have found that:

GMDD
6, 6775–6834, 2013

- In the clear sky test cases there is a consistent bias of +4 % to +6 %. This could be fixed by tuning the scheme.
- The cloud liquid transmittance formula currently used in hlradia performs impressively well, especially considering the simplicity of the hlradia parametrization.
- The cloud ice transmittance calculated with hlradia is within 10 % of that calculated with DISORT when the cloud ice load is less than 0.5 $\mathrm{kg\,m^{-2}}$. In the calculations ice clouds are assumed to consists of hexagonal columns.
- Assuming a constant ozone SW absorptance induces an error of a few percent at most.

Based on the above we propose the following future work:

- The current choice of 6 spectral bands in HARMONIE/IFS should be re-assessed, as the first spectral band is irrelevant for NWP modelling.
- The SW cloud inhomogeneity factor should be changed from 0.7 (0.8) to 1.0 in all schemes applied in HARMONIE.
- The effects on the general 3-D NWP results of using the Nielsen cloud liquid optical property parametrization within the IFS scheme should be tested.
- In order to improve the delta-Eddington radiative transfer calculations, the possibility of using a variable Hopf q function should be investigated.
- The hlradia gaseous transmission coefficients should be tuned to the DISORT clear sky results presented here.
- The impact of aerosols needs to be investigated further.

Acknowledgements. We acknowledge the support of the International HIRLAM-B Programme, the radiative transfer library libRadtran, and those who contributed their work to this library.

GMDD
6, 6775–6834, 2013

References

Anderson, G. P., Clough, S. A., Kneizys, F. X., Chetwynd, J. H., and Shettle, E. P.: AFGL Atmospheric Constituent Profiles (0–120 km), Tech. Rep. AFGL-TR-86-0110, Air Force Geophysics Lab Hanscom AFB, MA, USA, 1986. 6781, 6783

Baker, B. A. and Lawson, R. P.: In situ observations of the microphysical properties of wave, cirrus, and anvil clouds, Part I: Wave clouds, J. Atmos. Sci., 64, 3160–3185, 2006. 6792

Bass, A. M. and Paur, R. J.: The ultraviolet cross-sections of ozone: I. the measurements, in: Atmospheric Ozone, edited by: Zerefos, C. S. and Ghazi, A., 606–610, Springer, Netherlands, 1985. 6783

Bénard, P., Vivoda, J., Mašek, J., Smolaková, P., Yessad, K., Smith, C., R., B., and Geleyn, J.: Dynamical kernel of the Aladin–NH spectral limited-area model: revised formulation and sensitivity experiments, Q. J. R. Meteorol. Soc., 136, 155–169, 2010. 6777

Bhandari, A., Hamre, B., Frette, Ø., Zhao, L., Stamnes, J. J., and Kildemo, M.: Bidirectional reflectance distribution function of Spectralon white reflectance standard illuminated by incoherent unpolarized and plane-polarized light, Appl. Opt., 50, 2431–2442, 2011. 6790

Déqué, M., Dreveton, C., Braun, A., and Cariolle, D.: The ARPEGE/IFS atmosphere model: a contribution to the French community climate modelling, Clim. Dynam., 10, 249–266, 1994. 6777

Dobbie, J. S., Li, J., and Chýlek, P.: Two- and four-stream optical properties for water clouds and solar wavelengths, J. Geophys. Res., 104, 2067–2079, 1999. 6789

Ebert, E. E. and Curry, J. A.: A parameterization of ice cloud optical properties for climate models, J. Geophys. Res., 97, 3834–3836, 1992. 6779

ECMWF: IFS Documentation – Cy38r1, Part IV: Physical processes, available at: http://www.ecmwf.int/research/ifsdocs/CY38r1/IFSPart4.pdf (24 October 2013), 2012. 6777, 6786

Forster, P., Ramaswamy, V., Artaxo, P., Berntsen, T., Betts, R., Fahey, D. W., Haywood, J., Lean, J., Lowe, D. C., Myhre, G., Nganga, J., Prinn, R., Raga, G., Schultz, M., and Van Dorland, R.: Changes in Atmospheric Costituents and in Radiative Forcing, in: Climate Change 2007: The Physical Science Basis. Contribution of Working Group I to the Fourth Assessment Report of the Intergovernmental Panel on Climate Change, edited by: Solomon, S. S., Qin, D., Manning, M., Chen, Z., Marquis, M., Averyt, K. B., Tignor, M., and Miller, H. L., 129–234, Cambridge University Press, Cambridge, UK, 2007. 6776

GMDD
6, 6775–6834, 2013

Fouquart, Y.: Radiative transfer in climate modeling, in: NATO Advanced Study Institute on Physically-Based Modeling and Simulation of Climate and Climatic Changes, edited by: Schlesinger, M. E., 223–283, 1987. 6779, 6780, 6786, 6787, 6803, 6804, 6805
Fouquart, Y. and Bonnel, B.: Computations of solar heating of the earth's atmosphere – a new parameterization, Beitr. Phys. Atmos., 53, 35–62, 1980. 6779
Fu, Q.: An accurate parameterization of the solar radiative properties of cirrus clouds for climate models, J. Climate, 9, 2058–2082, 1996. 6776, 6779, 6791, 6792, 6793
Fu, Q. and Liou, K. N.: Parameterization of the radiative properties of cirrus clouds, J. Atmos. Sci., 50, 2008–2025, 1993. 6791, 6792, 6793
Hansen, J. E. and Travis, L. D.: Light scattering in planetary atmospheres, Space Sci. Rev., 16, 527–610, 1974. 6776
Hess, M., Köpke, P., and Schult, I.: Optical properties of aerosols and clouds, the software package OPAC, Bull. Am. Meteorol. Soc., 79, 831–844, 1998. 6776
Hogan, R. J. and Shonk, J. K. P.: Incorporating the effects of 3-D radiative transfer in the presence of clouds into two-stream multilayer radiation schemes, J. Atmos. Sci., 70, 708–724, 2013. 6788
Hopf, E.: Absorption lines and the integral equation of radiative equilibrium, Royal Astron. Soc., 96, 522–533, 1936. 6790
Hu, Y. and Stamnes, K.: An accurate parameterization of the radiative properties of water clouds suitable for use in climate models, J. Climate, 6, 728–742, 1993. 6776
Joseph, J. H., Wiscombe, W. J., and Weinman, J. A.: The Delta-Eddington approximation for radiative flux transfer, J. Atmos. Sci., 33, 2452–2459, 1976. 6779
Kahnert, M., Sandvik, A. D., Biryulina, M., Stamnes, J. J., and Stamnes, K.: Impact of ice particle shape on short-wave radiative forcing: a case study for an arctic ice cloud, J. Quant. Spec. Rad. Trans., 109, 1196–1218, 2008. 6777, 6792
King, J. I. F.: The Hopf *q* function simply and precisely evaluated, Astrophys. J., 132, 509–511, 1960.
King, J. I. F., Sillars, R. V., and Harrison, R. H.: Hopf *q* function evaluated to eight-digit accuracy, Astrophys. J., 142, 1655–1659, 1965.
Kurucz, R. L.: Synthetic infrared spectra, in: Infrared Solar Physics, IAU Symp. 154, edited by: Rabin, D. M. and Jefferies, J. T., Kluwer, Acad., Norwell, MA, USA, 1992. 6778
Lambert, J. H.: Lambert's Photometrie, Verlag von Wilhem Engelmann, Leipzig, Germany, 1760. 6790

GMDD
6, 6775–6834, 2013

Lawson, R. P., Baker, B. A., Pilson, B., and Mo, Q.: In situ observations of the microphysical properties of wave, cirrus, and anvil clouds, Part I: Cirrus clouds, J. Atmos. Sci., 63, 3186–3203, 2006. 6792

L'Ecuyer, T. S., Wood, N. B., Haladay, T., Stephens, G. L., and Stackhouse Jr., P. W.: Impact of clouds on atmospheric heating based on the R04 CloudSat fluxes and heating rates data set, J. Geophys. Res., 113, D00A15, doi:10.1029/2008JD009951, 2008. 6777

Lommel, E.: Die Photometrie der diffusen Zurückwerfung, Ann. Phys. U. Chem., 36, 473–502, 1889. 6790

Malardel, S., Lac, C., Pinty, J.-P., Thouron, O., Bouteloup, Y., Bouyssel, F., Seity, Y., and Nuissier, O.: Representation of clouds in AROME, in: Proceedings of the ECMWF Workshop on parametrization of clouds in large-scale models, ECMWF, Reading, UK, 2006. 6780

Manners, J., Vosper, S., and Roberts, N.: Radiative transfer over resolved topographic features for high-resolution weather prediction, Q. J. R. Meteorol. Soc., 138, 720–733, 2012. 6777

Martin, G. M., Johnson, D. W., and Spice, A.: The measurement and parameterization of effective radius of droplets in warm stratocumulus clouds, J. Atmos. Sci., 51, 1823–1842, 1994.

Mascart, P. J. and Bougeault, P.: The Meso-NH Atmospheric Simulation System: Scientific Documentation, Tech. rep., Meteo France, Toulouse, France, 2011. 6777, 6779, 6781, 6786, 6790

Mayer, B. and Kylling, A.: Technical note: The libRadtran software package for radiative transfer calculations - description and examples of use, Atmos. Chem. Phys., 5, 1855–1877, doi:10.5194/acp-5-1855-2005, 2005. 6777

Mie, G.: Beiträge zur Optik trüber Medien, speziell kolloidaler Metallösungen, Ann. Phys., 25, 377–445, 1908. 6779

Myhre, G., Bellouin, N., Berglen, T. F., Berntsen, T. K., Boucher, O., Grini, A., Isaksen, I. S. A., Johnsrud, M., Mishchenko, M. I., Stordal, F., and Tanre, D.: Comparison of the radiative properties and direct radiative effect of aerosols from a global aerosol model and remote sensing data over ocean, Tellus B, 59, 115–129, 2007. 6776

Nielsen, K. P.: Testing cloud parametrizations in NWP models against satellite data, HIRLAM Newsl., 58, 65–70, 2011. 6791

Oreopoulos, L., Mlawer, E., Delamere, J., Shippert, T., Cole, J., Fomin, B., Iacono, M., Jin, Z., Li, J., Manners, J., Räisänen, P., Rose, F., Zhang, Y., Wilson, M. J., and Rossow, W. B.: The continual intercomparison of radiation codes: results from phase I, J. Geophys. Res., 117, D06118, doi:10.1029/2011JD016821, 2012. 6777

GMDD
6, 6775–6834, 2013

Pierluissi, J. H. and Peng, G.-S.: New molecular transmission band models for LOWTRAN, Opt. Eng., 24, 541–547, 1985. 6776
Reddy, M. S., Boucher, O., Bellouin, N., Schulz, M., Balkanski, Y., Dufresne, J.-L., and Pham, M.: Estimates of global multicomponent aerosol optical depth and direct radiative perturbation in the Laboratoire de Météorologie Dynamique general circulation model, J. Geophys. Res., 110, D10S16. doi:10.1029/2004JD004757, 2005. 6776
Rodgers, C. D.: The radiative heat budget of the troposphere and lower stratosphere., Tech. Rep. A2, Dept. of Meteorology, Mass. Instit. Technology, Cambridge, MA, USA, 1967. 6784
Sagan, C. and Pollack, J. B.: Anisotropic nonconservative scattering and the clouds of Venus, J. Geophys. Res., 72, 469–477, 1967. 6776
Savijärvi, H.: Fast radiation parameterization schemes for mesoscale and short-range forecast models, J. Appl. Meteorol., 29, 437–447, 1990. 6778, 6780, 6781, 6784
Seity, Y., Brousseau, P., Malardel, S., Hello, G., Bénard, P., Bouttier, F., Lac, C., and Masson, V.: The AROME-France Convective-Scale Operational Model, Mon. Wea. Rev., 139, 976–991, 2011. 6777
Senkova, A., L.Rontu, and Savijärvi, H.: Parametrization of orographic effects on surface radiation in HIRLAM, Tellus A, 59, 279–291, 2007. 6776
Shettle, E. P.: Models of aerosols, clouds and precipitation for atmospheric propagation studies, in: Atmospheric Propagation in the UV, Visible, IR and mm-Region and Related System Aspects, 454, AGARD Conference Proceedings, 1989. 6776, 6781
Slingo, A.: A GCM parameterization for the shortwave radiative properties of water clouds, J. Atmos. Sci., 46, 1419–1427, 1989. 6779, 6780, 6787, 6789, 6804, 6805
Stamnes, K., Tsay, S.-C., Wiscombe, W., and Jayaweera, K.: Numerically stable algorithm for discrete-ordinate-method radiative transfer in multiple scattering and emitting layered media, Appl. Opt., 27, 2502–2509, 1988. 6777, 6784
Stamnes, K., Tsay, S.-C., and Laszlo, I.: DISORT, a General-Purpose Fortran Program for Discrete-Ordinate-Method Radiative Transfer in Scattering and Emitting Layered Media: Documentation and Methodology, Tech. rep., Stevens Insitute of Technology, Hoboken, NJ, USA, 2000. 6777, 6784
Tanré, D., Geleyn, J.-F., and Slingo, J.: First results of the introduction of an advanced aerosol-radiation interaction in the ECMWF low resolution global model, in: Aerosols and Their Climatic Effects, edited by: Gerber, H. E. and Deepak, A., 133–177, A. Deepak Publ., Hampton, VA, USA, 1984. 6781

GMDD
6, 6775–6834, 2013

Thomas, G. E. and Stamnes, K.: Radiative Transfer in the Atmosphere and Ocean, Cambridge University Press, New York, NY, USA, 2002. 6776, 6790

Undén, P.: Revised method of determination of the hybrid coordinate in HIRLAM, HIRLAM Newsletter, 56, 30–36, 2010. 6780

Undén, P., Rontu, L., Järvinen, H., Lynch, P., Calvo, J., Cats, G., Cuxart, J., Eerola, K., Fortelius, C., Garcia-Moya, J. A., Jones, C., Lenderlink, G., McDonald, A., McGrath, R., Navascues, B., Nielsen, N. W., Ødegaard, V., Rodriguez, E., Rummukainen, M., Rõõm, R., Sattler, K., Sass, B. H., Savijärvi, H., Schreur, B. W., Sigg, R., The, H., and Tijm, A.: HIRLAM-5 Scientific Documentation, Tech. rep., SMHI, norrköping, Sweden, 2002. 6777

Wiscombe, W. J.: Improved Mie scattering algorithms, Appl. Opt., 19, 1505–1509, 1980. 6779

Wyser, K., Rontu, L., and Savijärvi, H.: Introducing the effective radius into a fast radiation scheme of a mesoscale model, Contr. Atmos. Phys., 72, 205–218, 1999. 6778, 6780, 6792

GMDD

6, 6775–6834, 2013

Table 1. The benchmark radiative transfer experiments.

Experiment	Variable	Range
1	Integrated water vapour	0.32–32 $\mathrm{kg\,m^{-2}}$
2	Solar zenith angle	0–80°
3	Aerosols	on/off
4	Surface albedo (clear sky)	0.0–0.8
5	Cloud liquid water	0–5 $\mathrm{kg\,m^{-2}}$
6	Cloud drop eff. radius $r_{\mathrm{e,\ liq}}$	4–40 µm
7	Surface albedo (cloudy sky: (cloud water load 0.1 $\mathrm{kg\,m^{-2}}$)	0.0–0.8
8	Surface albedo (thick cloud: cloud water load 1.0 $\mathrm{kg\,m^{-2}}$)	0.0–0.8
9	Cloud ice (albedo=0.18)	0–0.5 $\mathrm{kg\,m^{-2}}$
10	Cloud ice (albedo=0.7)	0–0.5 $\mathrm{kg\,m^{-2}}$
11	$r_{\mathrm{e,\ ice}}$ (albedo = 0.18)	20–80 µm
12	$r_{\mathrm{e,\ ice}}$ (albedo = 0.7)	20–80 µm

GMDD
6, 6775–6834, 2013

Table 2. Coefficients used for the Nielsen liquid cloud optical parametrization. The columns show the wavelength bands (i) 2–6.

i	2	3	4	5	6
µm	0.25–0.44	0.44–0.69	0.69–1.19	1.19–2.38	2.38–4.00
a_i	1.606	1.638	1.685	1.77	1.87
b_i	1.015	1.019	1.024	1.035	1.046
c_i	1.000	1.000	0.99999	0.9985	0.823
d_i	3.3×10^{-8}	10×10^{-7}	1.49×10^{-5}	9.2×10^{-4}	0.004
e_i	0.868	0.868	0.867	0.864	0.886
f_i	1.4×10^{-4}	2.5×10^{-4}	3.1×10^{-4}	5.4×10^{-4}	0.0011
h_i	0.061	0.063	0.078	0.133	0.20
j_i	0.25	0.25	0.195	0.194	0.18

GMDD
6, 6775–6834, 2013

Table 3. Global radiation results for the aerosol experiment 3. The two last rows give the absolute and relative differences for the cases where aerosols were included/excluded for each of the three radiation schemes, respectively. Column 4 shows the relative differences between IFS and DISORT, column 6 shows the relative differences between hlradia and DISORT, each including or excluding their own aerosols.

Aerosols	DISORT	IFS		hlradia	
On	532	526	−1.0 %	555	+4.5 %
Off	558	565	+1.3 %	589	+5.5 %
Abs. diff.	−26	−38		−33	
Rel. diff.	−4.6 %	−6.8 %		−5.7 %	

GMDD
6, 6775–6834, 2013

Table 4. Absolute differences (unit: $W m^{-2}$) for experiment 5. IFS-F refers to the IFS radiation scheme using the Fouquart (1987) liquid cloud optical property parametrization. The numbers 0.7, 0.8 and 1.0 give the value of the cloud SW inhomogeneity factors.

Cl. wat. [$kg m^{-2}$]	IFS-F 0.7 diff.	IFS-F 1.0 diff.	hlradia 0.8 diff.	hlradia 1.0 diff.
0.000	−5.01	−5.01	23.99	23.99
0.001	8.72	6.02	40.38	40.38
0.002	12.56	7.61	51.22	51.22
0.005	24.66	14.11	63.34	53.19
0.010	41.67	23.70	68.76	51.37
0.020	60.75	32.02	68.86	42.55
0.050	72.20	27.93	50.26	16.27
0.100	65.88	16.65	32.03	0.52
0.200	48.20	4.83	19.98	−3.48
0.500	19.09	−6.76	11.80	−0.65
1.000	3.86	−9.34	8.28	1.37
2.000	−2.41	−7.80	5.83	2.19
5.000	−2.95	−3.76	3.59	2.09

GMDD
6, 6775–6834, 2013

Table 5. Absolute differences (unit: $W m^{-2}$) for experiment 5. IFS-F, IFS-S and IFS-N refer to the IFS radiation scheme using the Fouquart (1987), the Slingo (1989) and Nielsen liquid cloud optical property parametrization, respectively.

Cl. wat. [$kg m^{-2}$]	IFS-F diff.	IFS-S diff.	IFS-N diff.	hlradia diff.
0.000	−5.01	−5.01	−5.01	23.99
0.001	6.02	0.52	2.42	40.38
0.002	7.61	−1.94	1.38	51.22
0.005	14.11	−4.72	1.96	53.19
0.010	23.70	−6.28	4.38	51.37
0.020	32.02	−11.54	3.76	42.55
0.050	27.93	−27.48	−8.51	16.27
0.100	16.65	−33.70	−16.57	0.52
0.200	4.83	−27.82	−15.95	−3.48
0.500	−6.76	−14.28	−8.34	−0.65
1.000	−9.34	−8.48	−4.92	1.37
2.000	−7.80	−5.17	−3.48	2.19
5.000	−3.76	−2.01	−1.60	2.09

GMDD
6, 6775–6834, 2013

Table 6. Relative differences for experiment 6. IFS-F, IFS-S and IFS-N refer to the IFS radiation scheme using the Fouquart (1987), the Slingo (1989) and the Nielsen liquid cloud optical property parametrizations, respectively.

$r_{e,liq}$ [µm]	IFS-F % diff.	IFS-S % diff.	IFS-N % diff.	hlradia % diff.
4	17.13	−8.44	−11.01	2.02
7	10.52	−16.05	−10.64	−0.25
10	8.22	−16.65	−8.19	0.26
15	7.07	−13.99	−4.99	2.37
20	6.88	−10.01	−2.92	4.48
30	6.63	−1.06	−0.75	7.25
40	6.50	18.29	0.53	8.97

GMDD
6, 6775–6834, 2013

Table 7. As for Table 6 but for experiment 6 absolute differences in $W m^{-2}$.

$r_{e,\ liq}$ [µm]	IFS-F diff.	IFS-S diff.	IFS-N diff.	hlradia diff.
4	15.60	−7.69	−10.03	1.84
7	16.33	−24.90	−16.51	−0.38
10	16.65	−33.70	−16.57	0.52
15	18.15	−35.93	−12.81	6.09
20	20.18	−29.36	−8.56	13.16
30	22.59	−3.61	−2.55	24.73
40	24.08	67.75	1.95	33.22

GMDD
6, 6775–6834, 2013

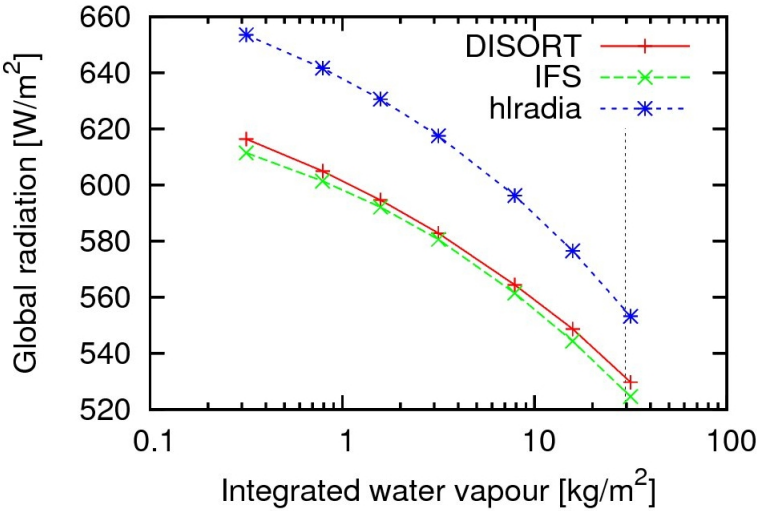

Fig. 1. Experiment 1: Global radiation as a function of integrated water vapour. The results from DISORT (red line with +), IFS (green line with x) and hlradia (blue line with *) are shown. The vertical dashed line marks the reference integrated water vapour used in the other experiments.

GMDD
6, 6775–6834, 2013

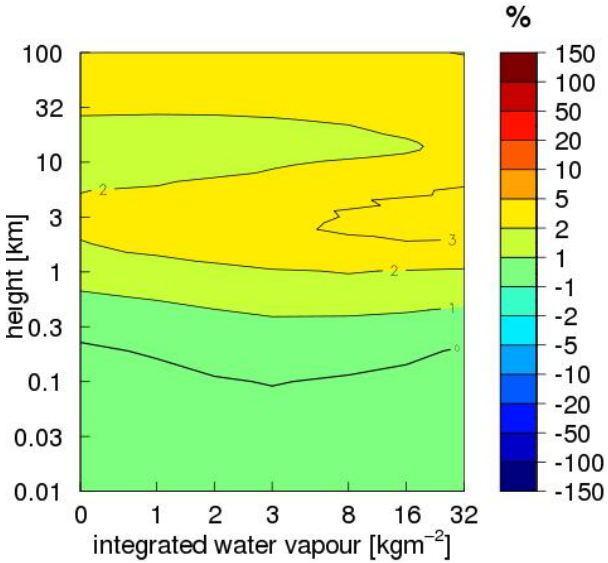

Fig. 2. Experiment 1: Relative differences (%) in net fluxes between the IFS radiation scheme and DISORT shown as a function of integrated water vapour and height.

GMDD
6, 6775–6834, 2013

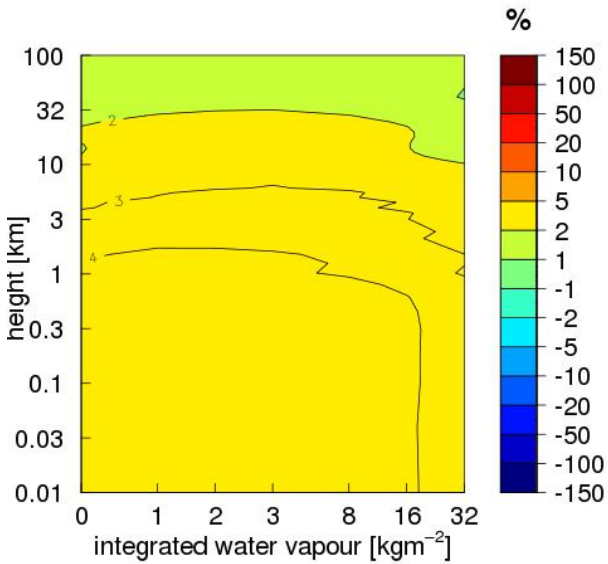

Fig. 3. As for Fig. 2 but for hlradia compared to DISORT.

GMDD
6, 6775–6834, 2013

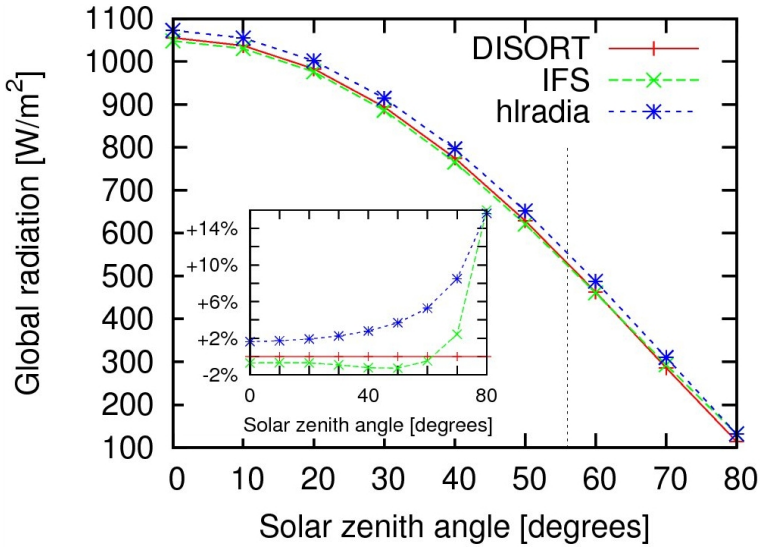

Fig. 4. As for Fig. 1 but for the solar zenith angle (experiment 2). The vertical dashed line marks the reference solar zenith angle used in the other experiments. The subplot shows the corresponding relative differences defined as (X-DISORT)/DISORT × 100 %.

GMDD
6, 6775–6834, 2013

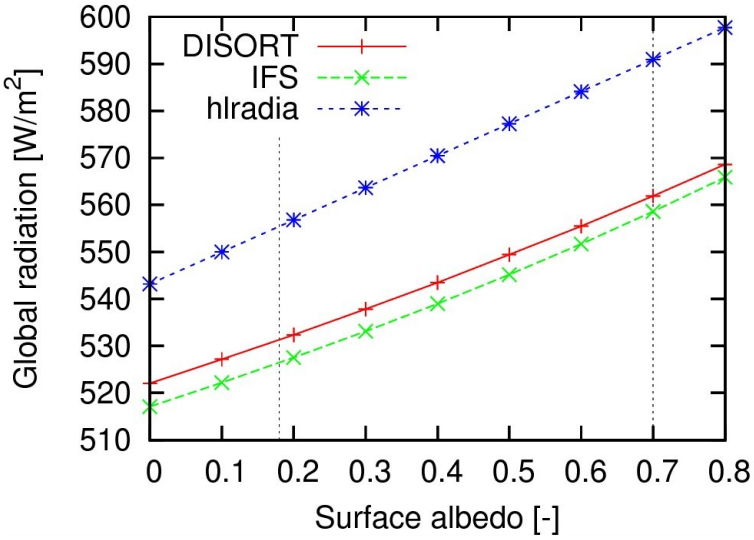

Fig. 5. As for Fig. 1 but for surface albedo (experiment 4). The vertical dashed line at 0.18 marks the reference albedo used in experiments 1–3, 5–6, 9 and 11. The vertical dashed line at 0.7 marks the albedo used in experiments 10 and 12.

GMDD
6, 6775–6834, 2013

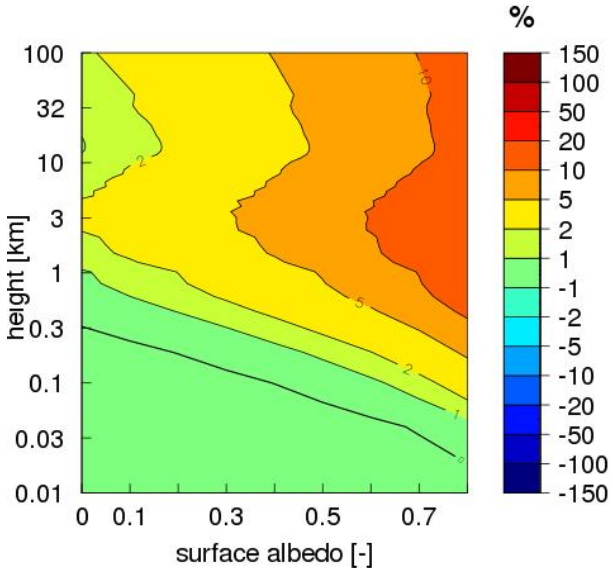

Fig. 6. As for Fig. 2 but for IFS-DISORT as a function of surface albedo (experiment 4).

GMDD
6, 6775–6834, 2013




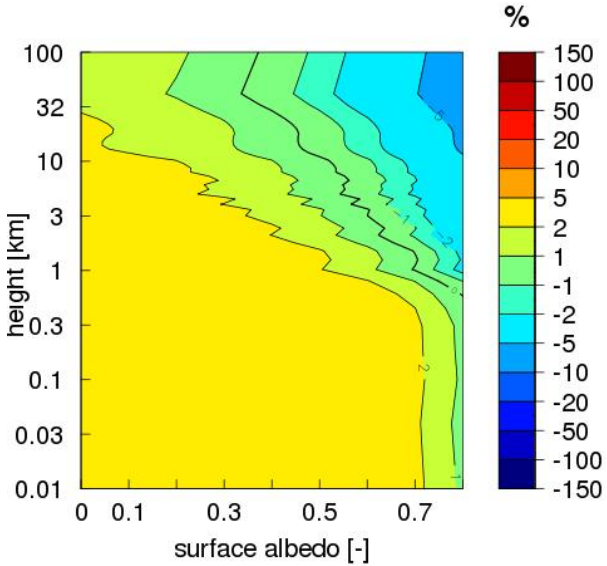

Fig. 7. As for Fig. 6 but for hlradia-DISORT.

GMDD
6, 6775–6834, 2013

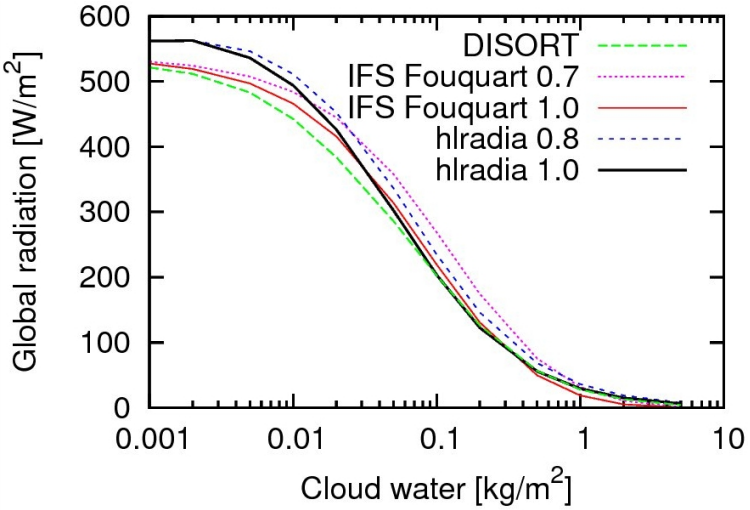

Fig. 8. Global radiation as a function of cloud water load (experiment 5). The results from DISORT (green dashed curve), IFS Fouquart with SW inhomogeneity factors of 0.7 (magenta dotted curve) and 1.0 (red curve), and hlradia with SW inhomogeneity factors of 0.8 (blue dashed curve) and 1.0 (black curve) are shown.

GMDD
6, 6775–6834, 2013

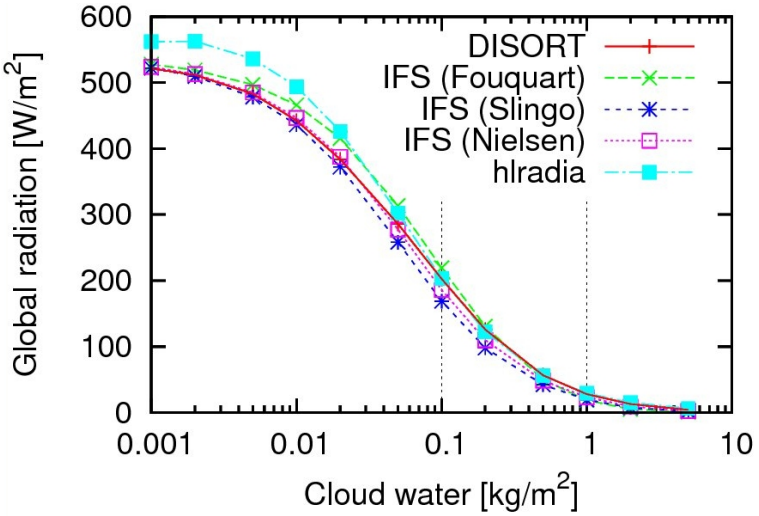

Fig. 9. As for Fig. 8 but here the SW inhomogeneity factor is 1.0 in all cases. The results for DISORT (red curve with +s), IFS Fouquart (green curve with xs), IFS Slingo (blue curve with *s), IFS Nielsen (magenta curve with boxes) and hlradia (cyan curve with filled boxes) are shown. The vertical dashed line at 0.1 kg m^{-2} marks the cloud water load used in experiments 6 and 7 while the other line at 1.0 marks that used in experiment 8.

GMDD
6, 6775–6834, 2013

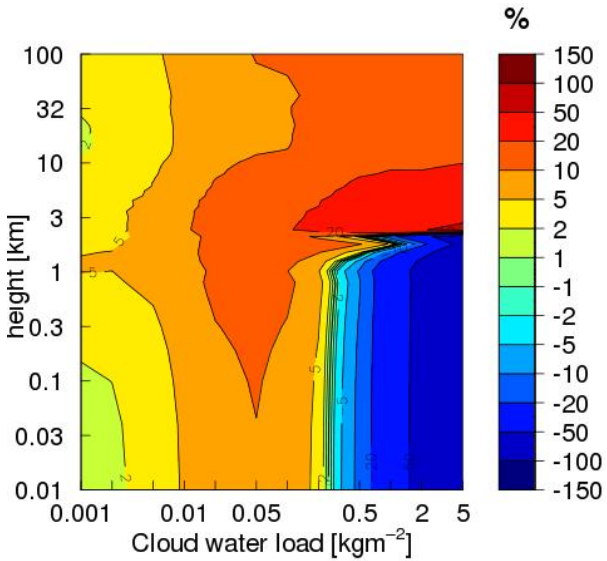

Fig. 10. As for Fig. 2 but for cloud water load and IFS-Fouquart vs. DISORT (experiment 5).

GMDD
6, 6775–6834, 2013

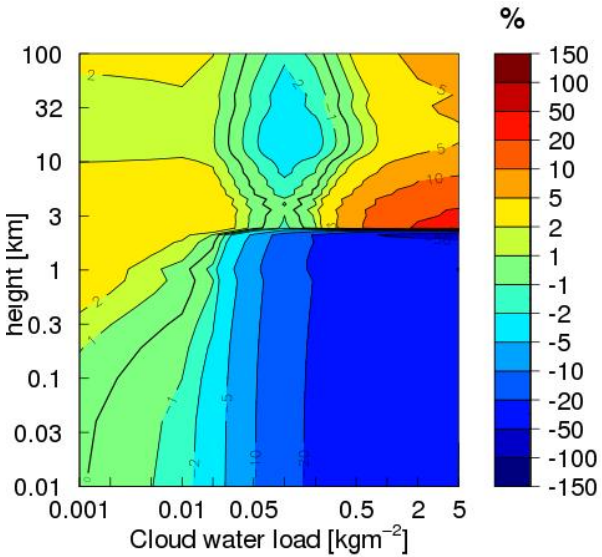

Fig. 11. As for Fig. 10 but for IFS-Slingo vs. DISORT.

GMDD
6, 6775–6834, 2013

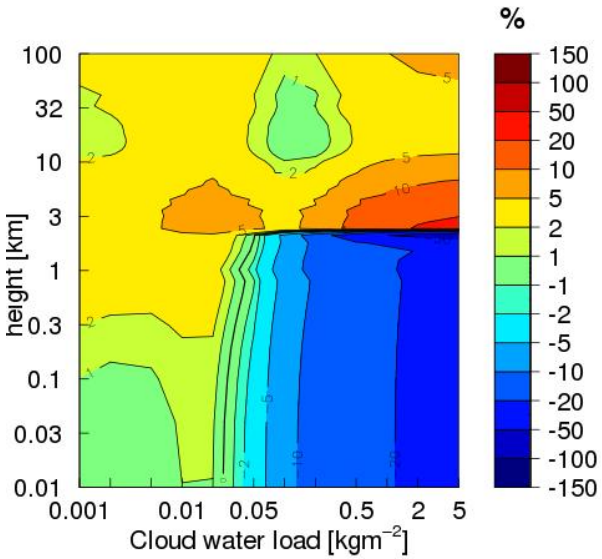

Fig. 12. As for Fig. 10 but for IFS-Nielsen vs. DISORT.

GMDD
6, 6775–6834, 2013

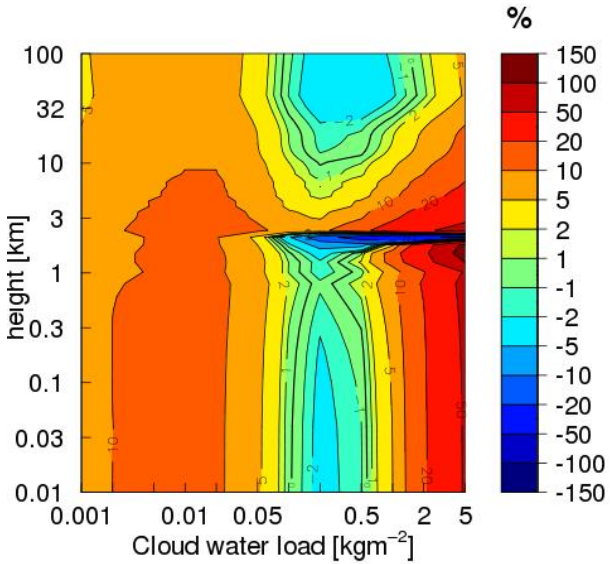

Fig. 13. As for Fig. 10 but for hlradia vs. DISORT.

GMDD
6, 6775–6834, 2013

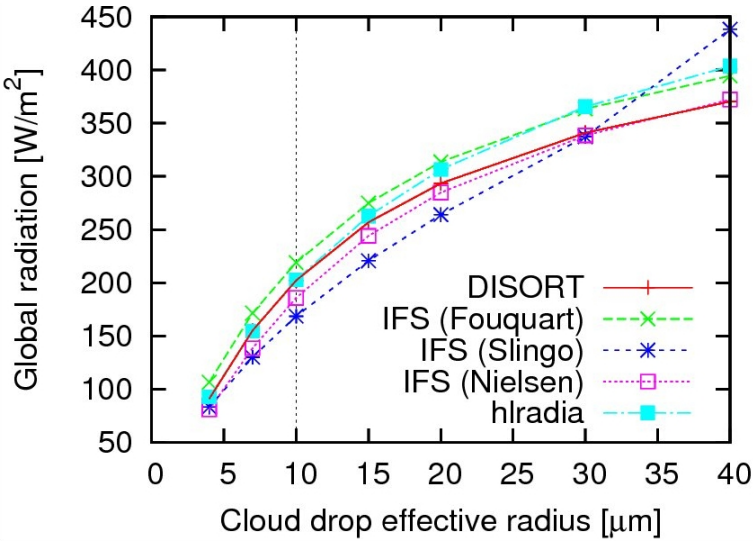

Fig. 14. As for Fig. 9 but for $r_{e,\,liq}$ (experiment 6). The vertical dashed line at 10 µm marks $r_{e,\,liq}$ used in experiments 5, 7 and 8.

GMDD
6, 6775–6834, 2013

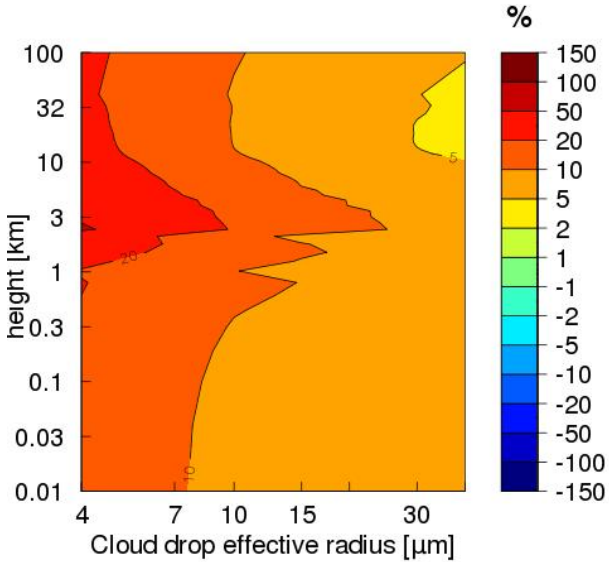

Fig. 15. As for Fig. 10 but for $r_{e,\,liq}$ (experiment 6). Relative differences in net fluxes between IFS-Fouquart and DISORT.

GMDD
6, 6775–6834, 2013

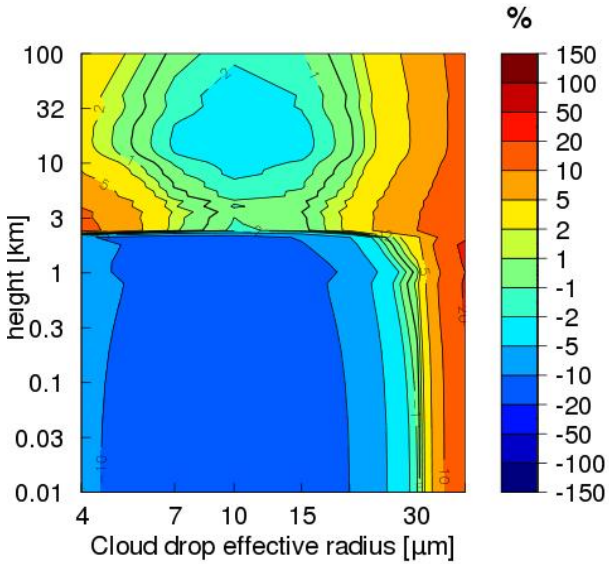

Fig. 16. As for Fig. 15 but for IFS-Slingo vs. DISORT.

GMDD
6, 6775–6834, 2013

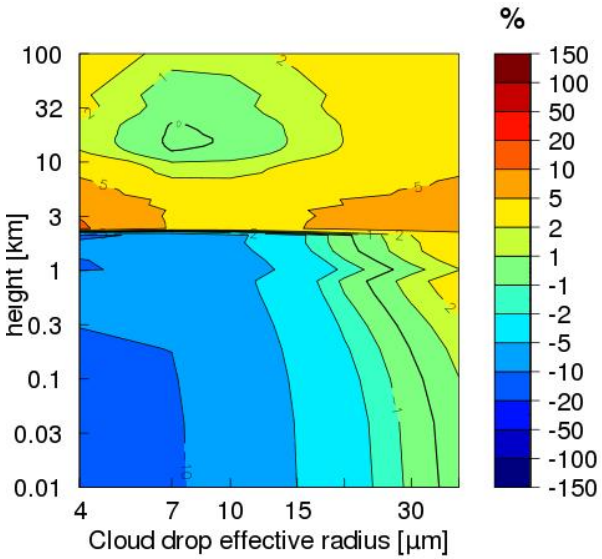

Fig. 17. As for Fig. 15 but for IFS-Nielsen vs. DISORT.

GMDD
6, 6775–6834, 2013

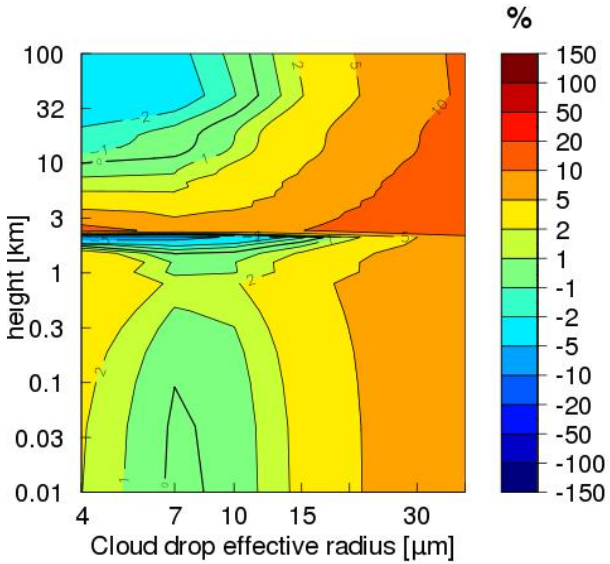

Fig. 18. As for Fig. 15 but for hlradia vs. DISORT.

GMDD
6, 6775–6834, 2013

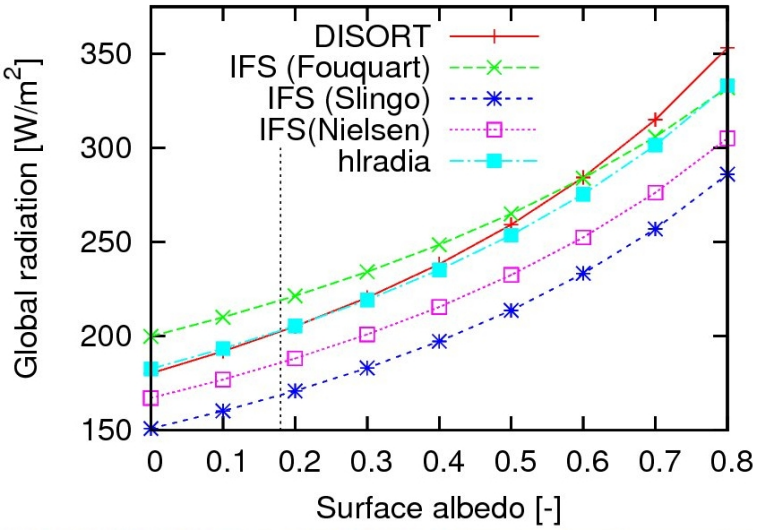

Fig. 19. As for Fig. 9 but for surface albedo for the case of a cloud of medium thickness (experiment 7). The vertical dashed line at 0.18 marks the reference albedo used in experiments 5 and 6.

GMDD
6, 6775–6834, 2013

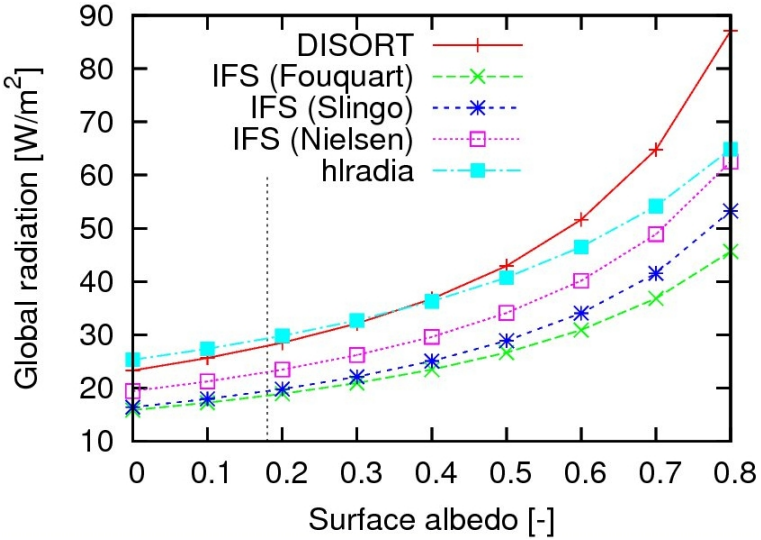

Fig. 20. As for Fig. 19 but for surface albedo for the case of a thick cloud (experiment 8).

GMDD
6, 6775–6834, 2013

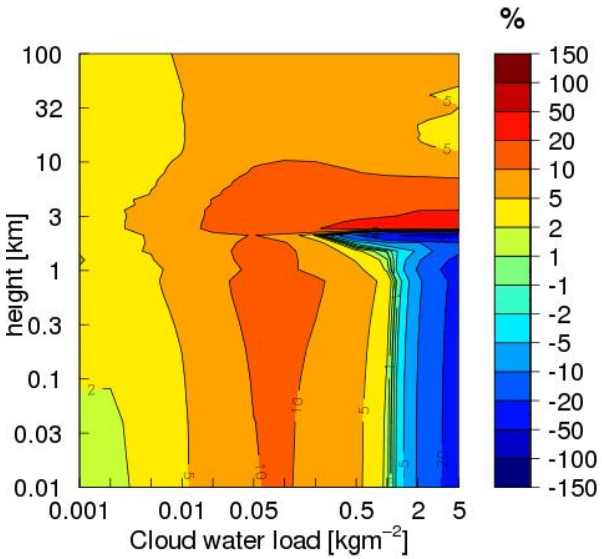

Fig. 21. As for Fig. 12 but run with the Hopf q function set to 71 %.

GMDD
6, 6775–6834, 2013

HARMONIE 37h1 radiation sensitivity tests

K. P. Nielsen et al.

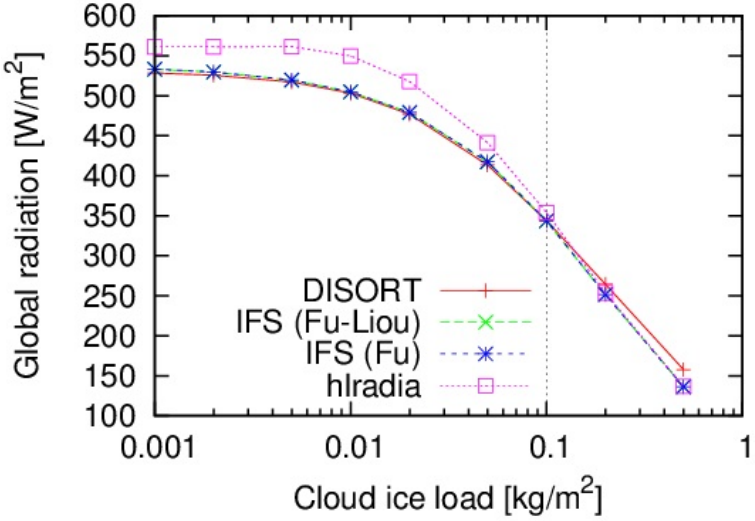

Fig. 22. As for Fig. 1 but for varying cloud ice load and fixed surface albedo = 0.18 (experiment 9). The vertical dashed line at 0.1 kg m^{-2} marks the cloud ice load used in experiments 11 and 12.

GMDD
6, 6775–6834, 2013

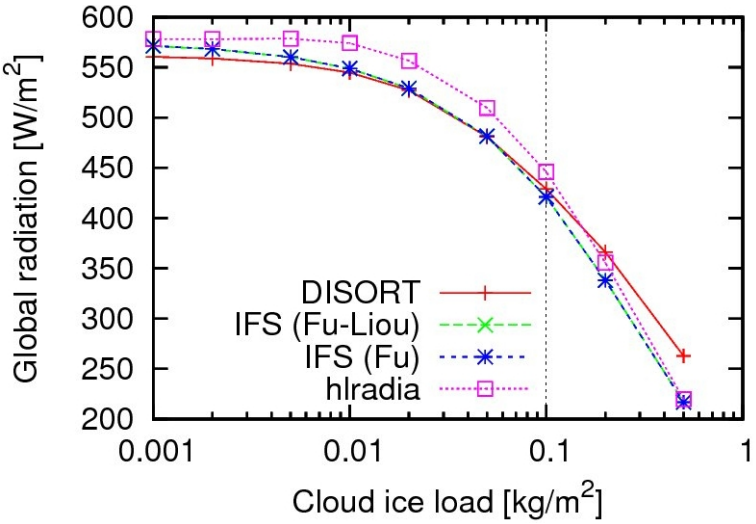

Fig. 23. As for Fig. 22 but for albedo = 0.7 (experiment 10).

GMDD
6, 6775–6834, 2013

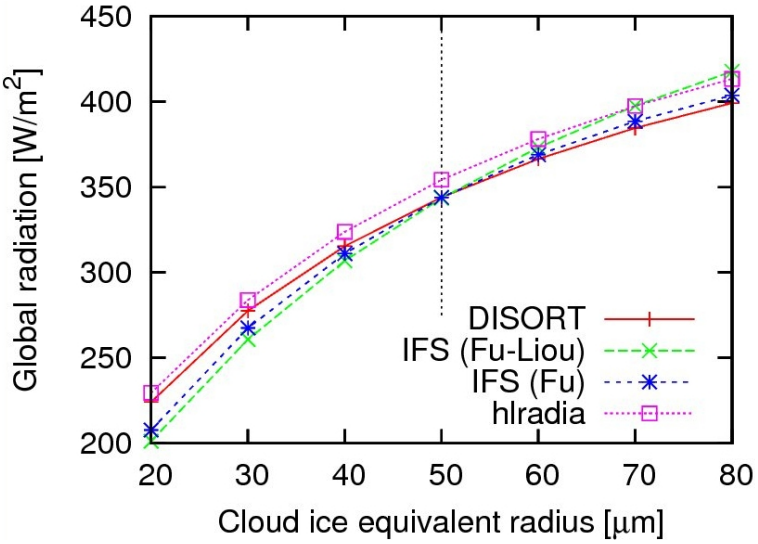

Fig. 24. As for Fig. 1 but for varying $r_{e,\ ice}$ and fixed albedo = 0.18 (experiment 11). The vertical dashed line at 50 µm marks the $r_{e,\ ice}$ value used in experiments 9 and 10.

GMDD
6, 6775–6834, 2013

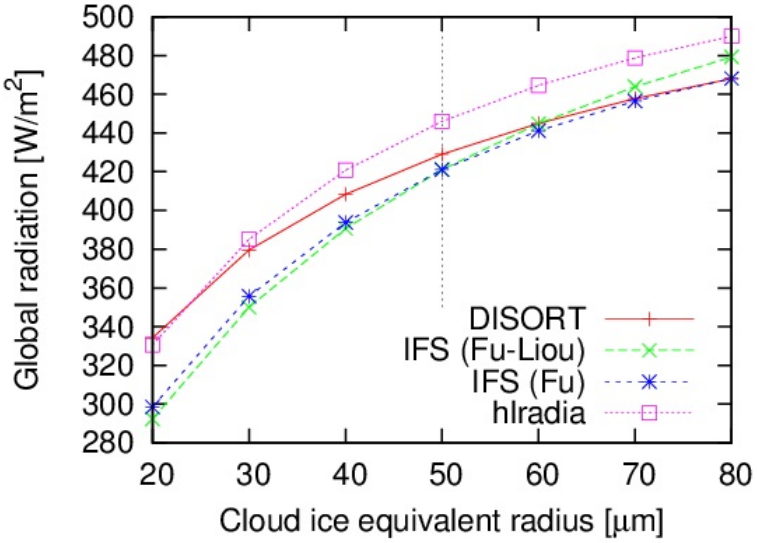

Fig. 25. As for Fig. 24 but for albedo = 0.7 (experiment 12).

GMDD
6, 6775–6834, 2013

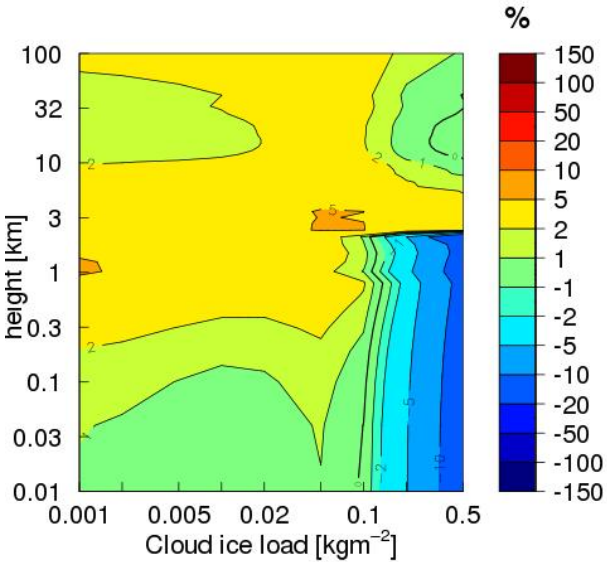

Fig. 26. As for Fig. 2 but for the IFS radiation scheme using the Fu and Liou (1993) ice cloud optical property parametrization vs. DISORT (experiment 9).

GMDD
6, 6775–6834, 2013

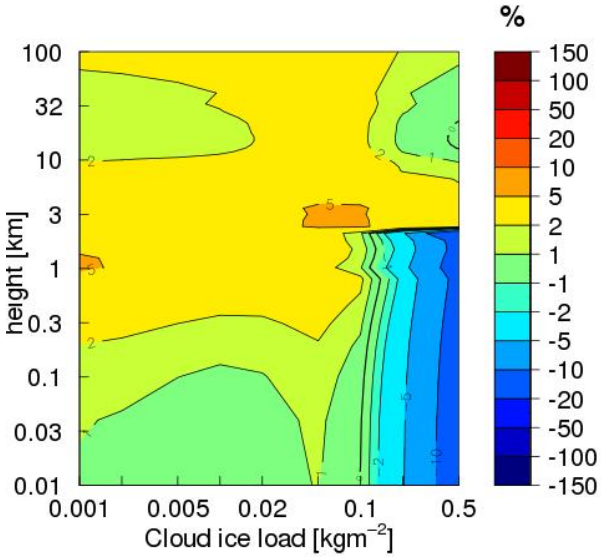

Fig. 27. As for Fig. 26 but for the IFS radiation scheme using the Fu (1996) ice cloud optical property parametrization vs. DISORT.

GMDD
6, 6775–6834, 2013

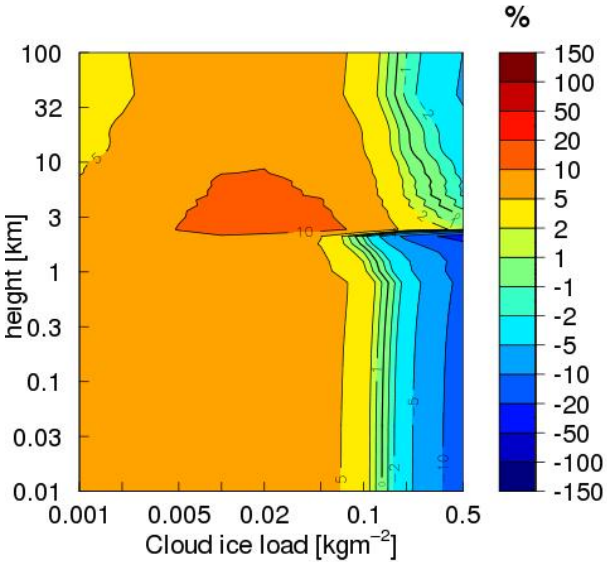

Fig. 28. As for Fig. 26 but for hlradia vs. DISORT.

GMDD
6, 6775–6834, 2013